PCCP

Accepted Manuscript

This is an *Accepted Manuscript*, which has been through the Royal Society of Chemistry peer review process and has been accepted for publication.

Accepted Manuscripts are published online shortly after acceptance, before technical editing, formatting and proof reading. Using this free service, authors can make their results available to the community, in citable form, before we publish the edited article. We will replace this *Accepted Manuscript* with the edited and formatted *Advance Article* as soon as it is available.

You can find more information about *Accepted Manuscripts* in the **Information for Authors**.

Please note that technical editing may introduce minor changes to the text and/or graphics, which may alter content. The journal's standard **Terms & Conditions** and the **Ethical guidelines** still apply. In no event shall the Royal Society of Chemistry be held responsible for any errors or omissions in this *Accepted Manuscript* or any consequences arising from the use of any information it contains.

www.rsc.org/pccp

Structures and Unimolecular Chemistry of

M(Pro$_2$-H)$^+$ (M=Mg, Ca, Sr, Ba, Mn, Fe, Co, Ni, Cu, Zn)

by IRMPD Spectroscopy, SORI-CID, and Theoretical Studies

Yasaman Jami-Alahmadi and Travis D. Fridgen

Department of Chemistry, Memorial University, St. John's, NL, Canada, A1B 3X7

1

Abstract

M(Pro$_2$-H)$^+$ complexes were electrosprayed and isolated in an FTICR cell where their unimolecular chemistries and structures were explored using SORI-CID and IRMPD spectroscopy. These experiments were augmented by computational methods such as electronic structure, simulated annealing, and atoms in molecules (AIM) calculations. The unimolecular chemistries of the larger metal cation (Ca^{2+}, Sr^{2+} and Ba^{2+}) complexes predominantly involve loss of neutral proline whereas the complexes involving the smaller Mg^{2+} and transition metal dications tend to lose small neutral molecules such as water and carbon dioxide. Interestingly, all complexes involving transition metal dications except for Cu(Pro$_2$-H)$^+$ lose H$_2$ upon collisional or IRMPD activation. IRMPD spectroscopy shows that the intact proline in the transition metal complexes and Cu(Pro$_2$-H)$^+$ is predominantly canonical (charge solvated) while for the Ca^{2+}, Sr^{2+}, and Ba^{2+} complexes, proline is in its zwitterionic form. The IRMPD spectra for both Mg(Pro$_2$-H)$^+$ and Mn(Pro$_2$-H)$^+$ are concluded to have contributions from both charge-solvated and canonical structures.

2
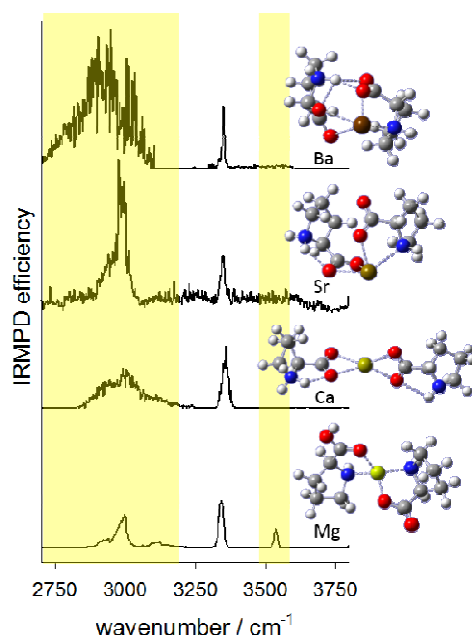
1. Introduction

Interactions between transition or alkali earth metal dications and biomolecules are of great interest and have garnered much attention due to the important roles they play in biological processes. Furthermore, it is anticipated that the detailed fundamental chemistry that can be learned from studying these small complexes will be transferrable to larger, more biologically relevant systems. Transition metals are present in trace amounts in living organisms complexed by peptides, proteins, or nucleic acids. The effects of metal cations can be positive, in fact necessary, stabilizing or binding substrates or acting as redox centres in enzyme catalyzed reactions; their effects can also be negative, destabilizing proteins or helical structures and acting as poisons. The nature of their effect depends on factors such as the identity of the metal cation or its concentration.[1]

The coordination of amino acids to transition metal ions has been studied in solution using techniques such as, X-ray diffraction, electron paramagnetic resonance (EPR),[2] optical absorption and FTIR studies,[2] HNMR,[3] UV-Vis spectroscopy,[3] and computational chemistry.[4,5] Gas-phase studies of metal-bound amino acid complexes have the advantage that the effects of counter ions and solvent can be eliminated. A more detailed understanding of the intrinsic physical chemistry of the ion/molecule complex can be obtained in the gas phase, providing a baseline to which solvent-phase experiments can be compared and provide information for models of metal ion-biomolecule interactions. IRMPD spectroscopy has proven to be one excellent tool to probe of the structures of amino acid bound metal ion complexes.[6,7,8,9,10,11,12,13,14,15,16,17,18,19,20] The positions of prominent modes, such as the C=O, N-H, and O-H stretch can shift significantly with changes in their bonding environment making this technique especially useful for the structural investigation of ionic amino acid complexes.

Proline is one of the twenty DNA-encoded amino acids and is unique in that its amine group is bound to its side chain making it a highly basic, secondary amine. Due to the ring structure of proline, when incorporated into a peptide or protein, it imparts a rigidity in the peptide backbone. For example, it has been proposed that a rate-limiting step in the protein folding is the cis/trans isomerization of the proteins that contain proline.[21] Recently in our lab, IRMPD spectroscopy and theory were used to conclude that the structure of the [Zn(Pro-H)]$^+$ complex in the gas phase can be described as an N/C2 or N/C5 dehydrogenated proline molecule (ie. Deprotonated at N and either C2 or C5 of proline) with ZnH$^+$ bound to

3

the imine N and carbonyl O. It was also found to predominantly lose neutral Zn upon collisional or IRMPD activation leaving the protonated dehydrogenated proline as the ionic product. Interestingly, the major fragmentation product for the "dimeric" $[Zn(Pro_2)-H]^+$ complex was found to be sequential double dehydrogenation unlike any of the primary amines studied. Sarcosine, another secondary amino acid, also underwent dehydrogenation.[22] To our knowledge this is the first report of dehydrogenation of a gas-phase amino acid complexes and one of the motivations of this study was to determine whether Zn^{2+} is unique or whether other $[M(Pro)_2-H]^+$ complexes would also dehydrogenate in the gas phase. Dehydrogenation of amino acids in biological systems occurs under the influence of amino acid oxidases using FAD as an oxidizing agent to dehydrogenate the substrate amino acid to the imino acid form. Following oxidation, the imino acid is transaminated to the alpha-keto acid.[23,24]

Transition metals in complexes can differ in terms of the metal oxidation state. To determine the geometry of transition metal bound ligand complexes, the degree of splitting of the d orbitals is significant and directs how orbitals can be filled and whether the complex is high spin vs low spin. Metals such as Mn, Fe, Co and Ni are capable of different d-orbital splitting and can adopt different possible spin states; this makes it more complicated to calculate all of the possible electronic geometries of these complexes.[25,26,27,28,29] The cooperation between mass spectrometry techniques and density functional theory (DFT) calculations would allow gaining some understanding on the structural information of amino acid bound metals that, in principle, may be useful to rationalize the behaviour of more complicated systems which present similar basic sites.

In this work we explore the unimolecular fragmentation pathways of the $[M(Pro)_2-H]^+$ complexes initiated by sustained off-resonance irradiation collision-induced dissociation (SORI-CID) in a Fourier transform ion cyclotron resonance (FTICR) mass spectrometer. We also present IRMPD spectroscopy in the $2700 - 3800 \text{ cm}^{-1}$ region, and for some complexes, in the $1000 - 1800 \text{ cm}^{-1}$ region which is backed by theory to help determine the structures of these $[M(Pro)_2-H]^+$ complexes.

2. Methodology

2.1. Experimental. All mass spectrometry experiments were performed using a Bruker ApexQe 7.0 FTICR. $[M(Pro)_2-H)]^+$ (M = Mn, Fe, Co, Ni, Cu, Zn, Mg, Ca, Sr, and Ba) ions were

formed by electrospray ionization (ESI) of 1 mL of 10 mmol L^{-1} aqueous solution of proline to which 15 μL of 10 mmol L^{-1} aqueous transition metal salt or 5 μL of the aqueous alkali earth metal salt were added. ESI was done with an Apollo II ESI source using a syringe pump operated at 100 μL h^{-1}. $MnCl_2$, $FeCl_2$, $Co(NO_3)_2$, $NiCl_2$, $CuCl_2$, $ZnCl_2$, $MgSO_4$, $CaCl_2$, $SrCl_2$,and $BaCl_2$ were the source of metal dications used in these experiments.

For SORI-CID experiments, the ions of interest were first isolated in the ICR cell then accelerated into argon gas under multiple collision SORI conditions. SORI/CID was completed inside the ICR cell which was followed by an Ar pulse to a pressure of ~10^{-6} mbar. SORI powers were applied in the range of 0.19–1.40 eV for 250 ms.

IRMPD experiments were performed by using two setups. IRMPD spectra in the 2700 – 4000 cm^{-1} region were obtained in the Laboratory for the Study of the Energetics, Structures, and Reactions of Gaseous Ions at Memorial University using an FTICR coupled to an IR OPO, manufactured by LaserSpec. This laser is tuneable from 1.4 to 4.5 μm, with a bandwidth of 2 cm^{-1}. The OPO, built around a periodically poled $LiNbO_3$ crystal, is pumped by a diode pumped solid state Nd:YAG laser. The OPO operates at 20 kHz, with pulse duration of few nanoseconds and generates output power near 3 W at 3 μm, however, the power was limited to 1 Watt in the present experiments. For IRMPD spectra in the fingerprint region an FTICR was coupled to a mid-infrared free electron laser (FEL)[30] with a 5 cm^{-1} bandwidth at the Centre Laser Infrarouge d'Orsay (CLIO). IRMPD irradiation times were between 1 and 2 seconds. The experimental IRMPD spectra were obtained by plotting the IRMPD efficiency (negative logarithm of the complex intensity divided by the total ion intensity) as a function of the radiation wavenumber. No attempts were made to correct the IRMPD spectra for fluctuations in laser power.

2.2. Computational methods. All calculations were performed using Gaussian 09.[31] Since all the transition metals studied here, except zinc, have unpaired electrons in their valence shells, the unrestricted open shell version of the B3LYP method (UB3LYP) was used. For Zn, which is a full d-shell orbital, and the alkali metals the restricted B3LYP was used. Geometry optimizations and calculations of the infrared spectra for the optimized structures were carried out using the 6-31+G(d,p) basis set on all atoms except for Sr and Ba, for which the Def2SVP basis sets were used. Empirical correction for dispersion was done using Grimme's D3 version with the original D3 damping function, B3LYPD3.[32] All harmonic frequencies were

corrected using scaling factors of 0.98 and 0.955 in the fingerprint and C-H/N-H/O-H stretching regions, respectively. These scaling factors are typical for the complexes of complexes and regions studied. Computed IR spectra were convoluted using Gaussian functions with a 10 cm-1 width (fwhm). Electronic energies were refined with single point calculations using B3LYPD3/6-311+G(3df,3pd) for all atoms except Sr and Ba for which the Def2TZVP basis sets were used. Just for comparison, geometry optimizations and frequency calculations were done using B3LYPD3 in with the cc-pVTZ basis set on some of the Co, Mn, and Mg complexes.

The bonding within the lowest-energy structures was analyzed by locating the bond critical points (BCPs) using atoms-in-molecules (AIM) theory,[33] which is based on a topological analysis of the electronic density at the BCPs, and is a good descriptor of the bond strength or weakness. This analysis was conducted using AIMAll software.[34]

3. Results and Discussion

3.1. SORI/CID of $[M(Pro)_2-H]^+$

3.1.1 M = Mn, Fe, Co, Ni, and Cu. As depicted in Figure 1, all the $[M(Pro)_2-H]^+$ complexes containing doubly charged first row transition metals, except Cu, were found to lose H_2, H_2O, and CO_2 as the primary fragmentation pathways upon SORI activation. The Zn complex was found to undergo the same primary fragmentation processes.[22] The MS/MS spectra for the $[M(Pro)_2-H]^+$ complexes where M=Mn, Fe, Co, and Ni are in Figures S1-S4, respectively, and confirm the three primary fragmentation pathways. The SORI mass spectra and MS/MS spectra also reveal secondary fragmentations which include further H_2 losses. $[Mn(Pro)_2-H]^+$ and $[Fe(Pro)_2-H]^+$ also lose a second CO_2 molecule. Interestingly, $[Co(Pro)_2-H]^+$ and $[Ni(Pro)_2-H]^+$ seem to not lose a second CO_2, but formic acid, HCOOH, instead. While this loss of 46 Da could originate from a loss of CO_2 followed by H_2 loss, or vice versa, MS/MS experiments were not able to reveal the ion resulting in two CO_2 losses. However, the MS/MS on some CO_2 loss products which were also dehydrogenated were indeed found to lose CO_2. For example, the ion at *m/z* 240 in the SORI spectrum of $[Co(Pro)_2-H]^+$ is the result of double dehydrogenation and loss of CO_2. When isolated and subjected to SORI-CID, *m/z* 240 was found to produce fragment ions resulting from loss of 44 and 46 Da (Figure S3). HCOOH is apparently a neutral loss, rather than loss of CO followed by loss of H_2O or vice versa. In Figure S1, for example, $Mn(Pro_2-H)^+$ loses H_2O to form 266 and also forms 238 loss of 46 Da.

However, 266 does not lose 28 Da, ruling out sequential H_2O + CO loss. No CO loss was observed for these complexes; this indicates but does not prove that CO loss followed by H_2O loss does not occur.

$[Cu(Pro)_2-H]^+$ (*m/z* 292) has a significantly different unimolecular chemistry—it was found to undergo loss of CO_2 as its sole primary dissociation producing *m/z* 248. MS/MS studies (Fig. S5) show that this primary loss of CO_2 is followed mainly by loss of HNCO, forming *m/z* 205 as well as a minor loss of H_2O. The fragment ion at *m/z* 205 was found to lose HCOOH.

It is worthwhile noting that none of these complexes lose proline, clearly due to very strong metal-proline interactions. Also, the fragmentation patterns and extent of fragmentations—no loss of N in any fragmentation except for secondary HNCO loss in $[Cu(Pro)_2-H]^+$—signifies strong metal-N binding in the complexes.

3.1.2 M = Mg, Ca, Sr, and Ba. The SORI-CID spectra for $[M(Pro)_2-H]^+$, where M are the alkaline earth metals are shown in Figure 2. The Sr and Ba complexes were found to primarily undergo loss of proline as their main fragmentation, although $[Sr(Pro)_2-H]^+$ underwent a small amount of successive H_2O loss as seen by fragment ions at *m/z* 299 and 281. $[Ca(Pro)_2-H]^+$ also underwent a significant amount of proline loss, but loss of H_2O strongly competes. A small amount of HCOOH loss is also observed for $[Ca(Pro)_2-H]^+$. MS/MS (Fig. S7) confirms that the ion at *m/z* 207 is a secondary loss of CO_2 following H_2O loss. Interestingly, following the loss of proline, $[Ca(Pro-H)]^+$ was seen to exhibit H_2 loss.

The main primary fragmentation observed for $[Mg(Pro)_2-H]^+$ (*m/z* 253) was loss of water with a small peak also observed for loss of HCOOH at *m/z* 207 as seen from the MS/MS data in Figure S6. The fragment ion at *m/z* 217 is due to a second water loss from *m/z* 235. The small peaks at *m/z* 205, 191, and 189 are due to secondary losses of H_2CO, CO_2 and HCOOH, respectively.

The trend in the fragmentation patterns observed for the alkali earth metal are expected if the binding to the metal cation was electrostatic. The larger Ba^{2+}, with less charge density binds less strongly to proline resulting in its loss. The smaller the central cation, the higher the charge density and the stronger the metal to proline interaction resulting in fragmentation of the proline ligand. The binding in $[Mg(Pro)_2-H]^+$ is so strong

that, like the transition metal cation complexes, which have a similarly small size and high charge density, no loss of proline and only proline fragmentation is observed.

3.2. IRMPD Spectroscopy of [M(Pro)$_2$-H]$^+$

3.2.1 M = Mn, Fe, Co, Ni, Cu and Zn. The experimental IRMPD spectra in the 2700–3800 cm^{-1} and 1000–1850 cm^{-1} for [M(Pro)$_2$-H]$^+$, (M = transition metal) are depicted in Figures 3 a) and b), respectively. The spectra for all transition metals contain absorptions above 3550 cm^{-1} and about 3370 cm^{-1} corresponding to a carboxylic acid O–H stretch and a free N-H stretch, respectively. The presence of the O-H stretch in the IRMPD spectrum clearly indicates structures in which one of the prolines has an intact carboxylic acid group—not deprotonated and non-zwitterionic. Weak bands below 3000 cm^{-1} can be ascribed to C-H stretching. In the fingerprint region, 1000–1850 cm^{-1}, for the metals we have spectra for, each have two bands between 1650 cm^{-1} and 1800 cm^{-1} assigned to the C=O stretching of two different carbonyl groups, one free (~1780 cm^{-1}) and one that has been weakened by a an interaction, probably with the metal cation (~1660 cm^{-1}). Also there is a set of pronounced features at around 1230 cm^{-1} in the region corresponding to modes such as COH bending, as well as CH$_2$ rocking. The spectrum in the fingerprint region for [Mn(Pro)$_2$-H]$^+$ is clearly different than the rest. It contains an intense band at 1450 cm^{-1} that could correspond to C-COO stretching and HNC bending as well as a pronounced shoulder at about 1620 cm^{-1} that could be assigned to NH$_2$ scissoring motions. The intense 1330 cm^{-1} band is also unique to Mn(Pro)$_2$-H]$^+$.

3.2.2 M = Mg, Ca, Sr and Ba. A comparison of the experimental IRMPD spectra in the 2800-3800 cm^{-1} region for the [Mg(Pro)$_2$-H]$^+$, [Ca(Pro)$_2$-H]$^+$, [Sr(Pro)$_2$-H]$^+$, and [Ba(Pro)$_2$-H]$^+$ complexes are displayed in Figure 3 c). The IRMPD spectra of the [Mg(Pro)$_2$-H]$^+$ complex is similar to the transition metal-bound complexes, containing absorptions corresponding to a free N–H stretch as well as an O–H stretching vibration, along with C-H stretching observed below 3000 cm^{-1}. Interestingly, the complexes where M = Ca, Sr or Ba do not have the O-H stretching band, only show the free N-H stretching feature corresponding to the zwitterionic form of proline at 3370 cm^{-1}. There are also very strong and broad bands below 3200 cm^{-1}, that are indicative of hydrogen bonded N-H or O-H stretches.

3.3. [M(Pro)$_2$-H]$^+$ Structures and Comparison of Computed IR Spectra to IRMPD Spectra

Based on our calculations, [M(Pro)$_2$-H]$^+$ consists of a deprotonated proline and an intact proline, the latter of which could adopt either a canonical or zwitterionic form, both coordinated to the metal cation. The carboxylic acid is the most acidic site in proline and is the site of deprotonation in these M(Pro$_2$-H)$^+$ complexes. The [M(Pro)$_2$-H]$^+$ complexes can adopt one of four main groupings of structural isomers as depicted in Scheme 1. The first label (NO or OO) describes the coordination of the intact proline to the metal cation and the second corresponds to binding of the deprotonated proline. The third label, CS or ZW, corresponds to canonical (charge solvated) or zwitterionic intact proline. First, NO-NO-CS structures are those where the metal cation is coordinated to N and an O atom of the carboxylic acid group of both canonical intact proline and the N and one of the O atoms of the carboxylate group of deprotonated proline. In the NO-OO-CS structures the metal cation is also bound through N and carbonyl-O of the canonical proline and both oxygens of the carboxylate group of deprotonated proline. In the third general group of structures, OO-OO-ZW, both zwitterionic proline and deprotonated proline are bound through the carboxylate oxygens. Finally, in OO-NO-ZW zwitterionic proline is bound through both carboxylate oxygens and deprotonated proline is bound through one carboxylate O and N. As in a previous work on the protonated and sodiated dimers of proline,[20] the same expression for the ring puckering type as outlined by Marino *et al.*[35] are used, E for endo, and X for exo puckering. The first label in the name corresponds with intact proline, and the second corresponds to deprotonated proline.

3.3.1 M = Mn, Fe, Co, Ni, Cu and Zn. Cu^{2+} and Zn^{2+} each have one spin state, doublet and singlet, respectively. Cu^{2+} complexes are all square planar while Zn^{2+} structures all have tetrahedral coordination. Mn can potentially have a doublet, quartet, or sextet spin state, but the high spin sextet complexes are significantly lower in energy (Table S1). The lowest energy sextet complexes are tetrahedral whereas the doublets and quartet all optimized to be square planar. Similarly for Fe, the high spin quintet complexes are the lowest in energy (Table S2) and are all tetrahedral. In contrast, the lowest energy Co and Ni complexes are the low spin doublets and singlets, respectively (Tables S3 and S4), and form square planar complexes. For Co, the quartet OO-NO-ZW, NO-OO-CS, and OO-OO-ZW complexes are lower in energy than the doublet. For Ni, the triplet OO-NO-ZW structures are lower in

energy than the singlet. All of the high spin Co and Ni complexes were computed to be tetrahedral and the low spin complexes were square planar. There is not as much difference in energy between the higher spin and lower spin states for the Co NO-NO-CS complexes as there is for the Ni, Mn, and Fe complexes, but the difference is enough (~10 kJ mol^{-1}) that only a discussion of the lowest energy NO-NO-CS spin states, in fact the lowest energy spin states for each of the four general structural isomer groups, will be discussed further.

The lowest energy structures for all [M(Pro)$_2$-H]$^+$ are NO-NO-CS and there is little difference in the energies of the different ring puckering conformers. As can be seen from Figure S10, for [Cu(Pro)$_2$-H]$^+$ and [Ni(Pro)$_2$-H]$^+$, the computed spectra for all four of the ring puckering conformers of the NO-NO-CS complexes are virtually identical and infrared spectroscopy could not be used to distinguish between them in either the N-H/O-H stretching or the fingerprint regions. In the discussions below we only compare the computed IR spectrum of the lowest energy conformer for each of the four structural isomer groups.

In Figure 4 the experimental spectra for both the [Zn(Pro)$_2$-H]$^+$ and [Cu(Pro)$_2$-H]$^+$ complexes in the 2700 – 3800 cm^{-1} range are compared to the computed IR spectra for the lowest energy structures of each of the four structural isomer groups. The positions of the experimental O-H, N-H, and C-H stretching vibrations are well- and best-reproduced by the computed spectra for the lowest energy NO-NO-CS structures. Also, in Figures 5, S17, and S18, the experimental spectra in both the fingerprint and 2700 – 3800 cm^{-1} regions are compared to computed IR spectra for [Co(Pro)$_2$-H]$^+$, [Fe(Pro)$_2$-H]$^+$, and [Ni(Pro)$_2$-H]$^+$, respectively. Once again, and in both regions of the infrared, the lowest energy NO-NO-CS structures best reproduced the experimental IRMPD spectrum.

As mentioned above, the experimental spectrum for [Mn(Pro)$_2$-H]$^+$ is more complex than the other transition metal complexes having intense bands at about 1330 and 1450 cm^{-1} and a strong shoulder at about 1620 cm^{-1}. In Figure 6, the experimental IRMPD spectrum is compared with the computed spectra for the lowest energy structure from each of the structural isomer groups. It is clear that the lowest energy NO-NO-CS structure does not account for the 1620, 1450, or 1330 cm^{-1} bands observed in the experimental spectrum. The NO-NO-CS structure also does not account for the observation that the N-H stretch is stronger than the O-H stretching band which is not observed for any of the other transition metal cation complexes. Calculations were done on each of the isomers shown in Figure 6,

where two water molecules were added to the complexes. The lowest energy structures found for each are shown in Figure S19 but most importantly, the energy of the solvated OO-OO-ZW structure is the lowest in energy, 13 kJ mol^{-1} lower than the NO-NO-CS structure. The grey spectrum underlying the experimental IRMPD spectrum is a simple sum of the computed IR spectra for the NO-NO-CS and OO-OO-ZW structures and better reproduces the experimental spectrum than either of the two individual computed spectra. Admittedly, the hydrogen bonded N-H stretch region is not well reproduced by the OO-OO-ZW complex, but this is expected for harmonic calculations. For comparison, the same solvation calculations were done on $[Cu(Pro)_2-H]^+$ (Figure S20) and while the energies of the zwitterionic structures did decrease slightly with respect to NO-NO-CS for the solvated complexes, they were still found to be significantly higher in energy, by 13 and 56 kJ mol^{-1}. The observation of both the charge solvated and zwitterionic structures for $[Mn(Pro)_2-H]^+$ is explained as being due to the zwitterionic structure being more stable when microsolvated. During the last stages of desolvation, the energy barrier for the zwitterionic to charge solvated structure is too high to surmount and the lowest energy, microsolvated zwitterionic $[Mn(Pro)_2-H]^+$ complex survives in the gas phase. It has been shown in the past that the last stages of solvation during electrospray, as well as the amount of energy imparted during desolvation can influence the structure of the gas phase ions observed.[36]

3.3.2 M = Mg, Ca, Sr and Ba. All computed structures for the $[M(Pro_2-H)]^+$ where M=Mg, Ca, Sr, and Ba are available in Figures S21-S24. All the Mg^{2+} complexes are tetrahedral about Mg^{2+}. The Ca^{2+} complexes are all tetrahedral except for the NO-OO-CS complexes which have a very distorted geometry for four coordinate species. All four interactions of the Ca^{2+} with the prolines occur on one hemisphere allowing for an apparent weak interaction between H on C5 of the intact proline and N of the deprotonated proline (2.5 Δ). Similar geometries for the Sr^{2+} and Ba^{2+} NO-OO-CS complexes were computed. The OO-OO-ZW structures for Sr^{2+} and Ba^{2+} take on an elongated tetrahedral shape. The OO-NO-ZW and NO-NO-ZW for both Sr^{2+} and Ba^{2+} and the NO-OO-CS for Ba^{2+} have a square pyramidal or distorted square pyramidal geometry with the metal cation at the apex, allowing the two prolines to interact with one another.

Only for $[Mg(Pro_2-H)]^+$ is the NO-NO-CS structure the lowest in energy, as was the case for the transition metal complexes. The OO-NO-ZW complex is only ~8 kJ mol^{-1} higher

in energy. The IRMPD spectrum for [Mg(Pro$_2$-H)]$^+$ is shown in Figure 7a and contains an O-H stretch, N-H stretch and C-H stretching bands, consistent with the computed spectrum for the NO-NO-CS structure. However, the broad band at about 3100 cm^{-1} and the significantly more intense N-H stretch compared to the O-H stretch is not reproduced. The second highest energy structure, OO-NO-ZW, does not have an O-H stretch because it is zwitterionic and there is a band predicted to occur at 3100 cm^{-1} due to a hydrogen bonded N-H stretch. Solvation calculations (Figure S25), like those done for the Mn^{2+} and Cu^{2+} complexes, reveal that the zwitterionic structures are significantly stabilized with respect to the charge solvated structures. In fact, the addition of solvent decreases the energy of OO-NO-ZW structure such that it is lower in energy by some 30 kJ mol^{-1}. As it was concluded for the Mn^{2+} complex, it is suggested that some of the solvent phase structure (OO-NO-ZW) survives the electrospray process and persist in the gas phase.

For [Ca(Pro$_2$-H)]$^+$, the lowest energy structure is the OO-OO-ZW structure. The IRMPD spectrum (Figure 7b) is consistent with that predicted for the OO-OO-ZW structure. The NO-OO-CS complex cannot be ruled out spectroscopically, but the absence of an O-H stretch in the IRMPD spectrum does rule out the charge-solvated structures. The intense broad band observed between 2800 and 3200 cm^{-1} is consistent with hydrogen bonded N-H stretching. The computed hydrogen bonded N-H and O-H stretching bands generally agree with the strong red shifting from the non-hydrogen bonded N-H and O-H stretches that is observed in the experimental spectra, but due to the harmonic nature of the calculations, they do not reproduce the broadness of the observed bands.

For [Sr(Pro$_2$-H)]$^+$ and [Ba(Pro$_2$-H)]$^+$, the lowest energy structures are found to be OO-NO-ZW. The computed IR spectra for the zwitterionic complexes are consistent with the IRMPD spectra for both (Figures 7c and 7d). As was the case for [Ca(Pro$_2$-H)]$^+$ the charge solvated structures are not observed due to the absence of O-H stretching features in the IRMPD spectra. The strong and broad features in the 3000 cm^{-1} region are consistent with N-H (or O-H) stretching vibrations that are strongly hydrogen bonded.[37,38] The behaviour, larger cations favouring the zwitterionic amino acid, have been observed before, for example in alkali metal cation complexes of histidine and threonine.[8,39]

3.3.3. 6-31+G(d,p) vs cc-pVTZ basis set. In Figures S27 – S29, Figures 5, 6, and 7a are reproduced only with the IRMPD spectra compared to spectra calculated using the cc-pVTZ

basis. These two basis sets produce almost identical results for the four isomers of the $M(Pro_2-H)^+$ (M=Co, Mn, Mg) complexes. Similarly the relative energies are compared in Tables S15 – S17. A comparison reveals no major differences in the computational methods used in this work for these complexes.

3.4. Metal-To-Proline Bonding: AIM Analysis.

In Tables S5-S14 are a summary of the AIM analyses done for the complexes studied in this work. For all of the complexes, the Laplacian of the charge density ($\Lambda^2\Delta$) is positive for all the metal to proline (O or N) interactions. The positive value of $\Lambda^2\Delta$ means a depletion of the charge density at the critical point suggesting closed shell or electrostatic interactions.

As discussed above, $[Mg(Pro_2-H)]^+$ behaves very much like the transition metals in both the CID and IRMPD spectroscopy experiments. Indeed these experimental findings are also consistent with electrostatic metal cation-to-ligand interactions. The larger and less-densely charged metal cations (Ca^{2+}, Sr^{2+}, and Ba^{2+}) exist as zwitterions and predominantly loose proline following collisional or IRMP activation. On the other hand, the smaller, and more densely charged transition metal and Mg^{2+} cations are more strongly bound to their ligands which are shown to fragment and the intact proline is predominantly in the charge solvated form in the complex. These findings are consistent with the results of the alkali earth metal dication/tryptophan[40] and phenylalanine[41] complexes where the larger metal cations were found to favour the zwitterionic structure. Similarly, alkali metal cationized complexes of arginine,[42,43] serine,[18] and methionine[44] showed a tendency toward zwitterionic structures as the metal cation increases in size. In contrast, the zwitterionic structures of aliphatic amino acids (including proline) were found to be stabilized by the smaller alkali metal cations.[45] This latter trend was convincingly explained using the principle hard and soft Lewis acids and bases; the smaller, harder metal cations prefer to bind to the harder carboxylate base while the larger, softer metal cations prefer to bind to the softer carbonyl.

The question, then, is how to explain the opposite trend in the present experiments where the zwitterionic proline structure is observed for the larger cations, Ca^{2+}, Sr^{2+}, and Ba^{2+} and the charge solvated structure is observed for the smaller cations. The principles of hard and soft Lewis acids and bases were developed based on observations of chemical

bonding in the condensed phase and included solvent contributions.[46] The results of the AIM analysis shows that the interaction between the metal cation and the ligands are all electrostatic in nature. Since the M(Pro-H)$^+$—Pro interactions are electrostatic, either ionic or ion-dipole interactions, the smaller more densely charged cations would favour an ion-dipole interaction between M(Pro-H)$^+$ and neutral proline which occurs in the charge-solvated complexes. Indeed, the M(Pro-H)$^+$ moiety is bound to canonical proline along its dipole. For the larger more polarizable cations, the ion-dipole complex is not as strong. So, to maximize bonding interactions and overall stablilization of the complex, the M(Pro-H)$^+$ cation interacts with the negative end of the zwitterionic neutral proline.

4. Conclusions and Final Comments

The unimolecular chemistries and structures of ten gas phase $[M(Pro_2)-H]^+$ complexes have been explored using a combination of SORI-CID, IRMPD spectroscopy, and computational methods. It was shown that the complexes containing the larger metal cations, Ca^{2+}, Sr^{2+}, and Ba^{2+} predominantly lose neutral proline. Furthermore, their structures are shown to have a zwitterionic neutral proline moiety. On the contrary, the complexes of Mg^{2+} and the transition metal dications tend to fragment losing small neutral molecules such as water and carbon dioxide. Furthermore, the neutral proline molecule in these complexes involving the smaller metal cations is canonical (or charge-solvated). The charge-solvation structures for the complexes involving the smaller cations are rationalized based upon the formation of strong ion-dipole complexes for these species. The larger cations do not make as strong an ion dipole complex. To maximize bonding they form strong "ionic" interactions between M(Pro-H)$^+$ and the negative end of the zwitterionic structure.

As a final comment, it was also shown, that upon collisional or IRMPD activation, all complexes involving transition metal dications *except* the one with the Cu^{2+} lose H_2 upon collisional or IRMPD activation. This was first observed for $[Zn(Pro_2)-H]^+$,[22] and a mechanism was proposed involving H transfer from C5 to Zn, followed by eventual elimination of H_2 from Zn and N, and that H_2 originates from the intact (not deprotonated) proline. The surprising observation that the Zn^{2+} complex is not alone in its ability to undergo H_2 elimination but rather the Cu^{2+} complex is alone (among the transition metals studied) in its inability to produce H_2. It is important to speculate as to why this might be. Neither IRMPD spectroscopy, nor the calculations reveal any unique structure for the Cu complex, so the

difference in reactivity is not due to a difference in the lowest energy structure. However, one unique property of copper, compared to the other transition metals explored in this study is its positive standard reduction potential (see Figure S26), meaning that compared to the other transition metals, copper prefers to keep its electrons. A comparable property in the gas phase is the ionization energy; copper has the highest second ionization energy of all the transition metals.   It is reasonable to assume that at some point during H_2 elimination electron density is required by proline, and Cu^{2+}, with a very high affinity for its electrons, does not readily accommodate the need for electron density to allow for H_2 elimination.

Acknowledgements

15

References

(1)   Duguid, J.; Bloomfield, V. a; Benevides, J.; Thomas, G. J. Raman Spectroscopy of DNA-Metal Complexes. I. Interactions and Conformational Effects of the Divalent Cations: Mg, Ca, Sr, Ba, Mn, Co, Ni, Cu, Pd, and Cd. *Biophys. J.* **1993**, *65*, 1916–1928.

(2)   Rani, P. N. V. V. L. P.; Chandra, J. S.; Parvathi, V.; Sunandamma, Y. Spectroscopic Investigations of Mn (II) Doped Ni L- Histidine Hydrochloride Monohydrate Crystals. **2013**, *3*, 3615–3620.

(3)   Waheed, E. J. Synthesis and Characterization of Some Metals Complexes of { N- [(Benzoyl Amino) -Thioxo Methyl] Proline }. **2012**, *15*, 1–10.

(4)   Rulíšek, L.; Havlas, Z. Theoretical Studies of Metal Ion Selectivity. 1. DFT Calculations of Interaction Energies of Amino Acid Side Chains with Selected Transition Metal Ions (Co2+, Ni2+, Cu2+, Zn2+, Cd2+, and Hg2+). *J. Am. Chem. Soc.* **2000**, *122*, 10428–10439.

(5)   Yang, G.; Zhu, R.; Zhou, L.; Liu, C. Interactions of Zn(II) with Single and Multiple Amino Acids. Insights from Density Functional and Ab Initio Calculations. *J. Mass Spectrom.* **2012**, *47*, 1372–1383.

(6)   Ziegler, B. E.; Marta, R. A.; Burt, M. B.; McMahon, T. B. Insight into the Gas-Phase Structure of a Copper(II) L-Histidine Complex, the Agent Used To Treat Menkes Disease. *Inorg. Chem.* **2014**, *53*, 2349–2351.

(7)   Aguilar-Galindo, F.; Montero-Campillo, M. M.; Yáñez, M.; Mó, O. On the Stability of [Pb(Proline)]2+ Complexes. Reconciling Theory with Experiment. *Chem. Phys. Lett.* **2014**, *598*, 91–95.

(8)   Citir, M.; Hinton, C. S.; Oomens, J.; Steill, J. D.; Armentrout, P. B. Infrared Multiple Photon Dissociation Spectroscopy of Cationized Histidine: Effects of Metal Cation Size on Gas-Phase Conformation. *J. Phys. Chem. A* **2012**, *116*, 1532–1541.

(9)   Corral, I.; Lamsabhi, A. M.; Mó, O.; Yáñez, M. Infrared Spectra of Charge-Solvated versus Salt-Bridge Conformations of Glycine-, Serine-, and Cysteine-Ca2+ Complexes. *Int. J. Quantum Chem.* **2012**, *112*, 2126–2134.

(10)   Drayss, M. K.; Blunk, D.; Oomens, J.; Scha, M. Infrared Multiple Photon Dissociation
        Spectroscopy of Potassiated Proline. **2008**, 11972–11974.

(11)   Yang, B.; Wu, R. R.; Polfer, N. C.; Berden, G.; Oomens, J.; Rodgers, M. T. IRMPD Action
        Spectroscopy of Alkali Metal Cation-Cytosine Complexes: Effects of Alkali Metal
        Cation Size on Gas Phase Conformation. *J. Am. Soc. Mass Spectrom.* **2013**, *24*, 1523–
        1533.

(12)   Fridgen, T. D. Infrared Consequence Spectroscopy of Gaseous Protonated and Metal
        Ion Cationized Complexes. *Mass Spectrom. Rev.* **2009**, *28*, 586–607.

(13)   Polfer, N. C.; Oomens, J. Vibrational Spectroscopy of Bare and Solvated Ionic
        Complexes of Biological Relevance. *Mass Spectrom. Rev.* **2009**, *28*, 468–494.

(14)   Eyler, J. R. Infrared Multiple Photon Dissociation Spectroscopy of Ions in Penning
        Traps. *Mass Spectrom. Rev.* **2009**, *28*, 448–467.

(15)   Bush, M. F.; Forbes, M. W.; Jockusch, R. A.; Oomens, J.; Polfer, N. C.; Saykally, R. J.;
        Williams, E. R. Infrared Spectroscopy of Cationized Lysine and ε-N-Methyllysine in the
        Gas Phase: Effects of Alkali-Metal Ion Size and Proton Affinity on Zwitterion Stability.
        J. Phys. Chem. A **2007**, *111*, 7753–7760.

(16)   Schmidt, J.; Kass, S. R. Zwitterion vs Neutral Structures of Amino Acids Stabilized by a
        Negatively Charged Site: Infrared Photodissociation and Computations of Proline-
        Chloride Anion. *J. Phys. Chem. A* **2013**, *117*, 4863–4869.

(17)   Atkins, C. G.; Rajabi, K.; Gillis, E. A. L.; Fridgen, T. D. Infrared Multiple Photon
        Dissociation Spectra of Proton- and Sodium Ion-Bound Glycine Dimers in the N–H and
        O–H Stretching Region. *J. Phys. Chem. A* **2008**, *112*, 10220–10225.

(18)   Armentrout, P. B.; Rodgers, M. T.; Oomens, J.; Steill, J. D. Infrared Multiphoton
        Dissociation Spectroscopy of Cationized Serine: Effects of Alkali-Metal Cation Size on
        Gas-Phase Conformation. *J. Phys. Chem. A* **2008**, *112*, 2248–2257.

(19)   Bush, M. F.; Oomens, J.; Saykally, R. J.; Williams, E. R. Effects of Alkaline Earth Metal
        Ion Complexation on Amino Acid Zwitterion Stability: Results from Infrared Action
        Spectroscopy. *J. Am. Chem. Soc.* **2008**, *130*, 6463–6471.

(20)   Jami-Alahmadi, Y.; Gholami, A.; Fridgen, T. D. The Protonated and Sodiated Dimers of
        Proline Studied by IRMPD Spectroscopy in the N-H and O-H Stretching Region and

Computational Methods. *Phys. Chem. Chem. Phys.* **2014**, *16*, 26855–26863.

(21)   Pappenberger, G.; Aygun, H.; Engels, J. W.; Reimer, U.; Fischer, G.; Kiefhaber, T. Nonprolyl Cis Peptide Bonds in Unfolded Proteins Cause Complex Folding Kinetics. *Nat Struct Mol Biol* **2001**, *8*, 452–458.

(22)   Gholami, A.; Fridgen, T. D. The Unimolecular Chemistry of [Zn(amino acid)2-H]+ in the Gas Phase: H2 Elimination When the Amino Acid Is a Secondary Amine. *Phys. Chem. Chem. Phys.* **2014**, *16*, 3134–3143.

(23)   Umhau, S.; Pollegioni, L.; Molla, G.; Diederichs, K.; Welte, W.; Pilone, M. S.; Ghisla, S. The X-Ray Structure of D -Amino Acid Oxidase at Very High Resolution Identifies the Chemical Mechanism of Flavin-Dependent Substrate Dehydrogenation. **2000**, *97*, 0–5.

(24)   Bruice, P. Y.; 1961/11/01, Y.-. *Amino Acid Metabolism*; p. Seven Edition.

(25)   Glatzel, P.; Bergmann, U. High Resolution 1s Core Hole X-Ray Spectroscopy in 3d Transition Metal Complexes—electronic and Structural Information. *Coord. Chem. Rev.* **2005**, *249*, 65–95.

(26)   Dunbar, R. C.; Steill, J. D.; Polfer, N. C.; Oomens, J. Dimeric Complexes of Tryptophan with M2+ Metal Ions. *J. Phys. Chem. A* **2009**, *113*, 845–851.

(27)   Turecek, F.; Jones, J. W.; Holm, A. I. S.; Panja, S.; Nielsen, S. B.; Hvelplund, P. Transition Metals as Electron Traps. I. Structures, Energetics, Electron Capture, and Electron-Transfer-Induced Dissociations of Ternary Copper-Peptide Complexes in the Gas Phase. *J. Mass Spectrom.* **2009**, *44*, 707–724.

(28)   Khodabandeh, M. H.; Davari, M. D.; Zahedi, M.; Ohanessian, G. Complexation of Glycine by Manganese (II) in the Gas Phase: A Theoretical Study. *Int. J. Mass Spectrom.* **2010**, *291*, 73–83.

(29)   Rimola, A.; Rodrı, L.; Sodupe, M. Cation - π Interactions and Oxidative Effects on Cu + and Cu 2 + Binding to Phe , Tyr , Trp , and His Amino Acids in the Gas Phase . Insights from First-Principles Calculations. **2006**, *9*, 24189–24199.

(30)   Prazeres, R.; Glotin, F.; Insa, C.; Jaroszynski, D. A.; Ortega, J. M. Two-Colour Operation of a Free-Electron Laser and Applications in the Mid-Infrared. *Eur. Phys. J. D* **1998**, *3*, 87–93.

(31)   Frisch, M. J.; Trucks, G. W.; Schlegel, H. B.; Scuseria, G. E.; Robb, M. A.; Cheeseman, J.
        R.; Scalmani, G.; Barone, V.; Mennucci, B.; Petersson, G. A.; *et al.* Gaussian 09,
        Revision B.01. *Gaussian 09, Revision B.01, Gaussian, Inc., Wallingford CT*, 2009.

(32)   Grimme, S.; Antony, J.; Ehrlich, S.; Krieg, H. A Consistent and Accurate Ab Initio
        Parametrization of Density Functional Dispersion Correction (DFT-D) for the 94
        Elements H-Pu. *J. Chem. Phys.* **2010**, *132*.

(33)   Bader, R. F. W. Atoms in Molecules: A Quantum Theory, Clarendon Press. *Oxford
        Univ. Press. Oxford, New York* **1990**.

(34)   AIMAll (Version 14.10.27), Todd A. Keith, TK Gristmill Software. *Overl. Park KS, USA,*
        2014, 10708–10711.

(35)   Marino, T.; Russo, N.; Tocci, E.; Toscano, M. Density Functional Computations of
        Proton Affinity and Gas-Phase Basicity of Proline. *J. Mass Spectrom.* **2001**, *36*, 301–
        305.

(36)   Rogalewicz, F.; Hoppilliard, Y.; Ohanessian, G. Structures and Fragmentations of
        zinc(II) Complexes of Amino Acids in the Gas Phase: IV. Solvent Effect on the Structure
        of Electrosprayed Ions. *Int. J. Mass Spectrom.* **2003**, *227*, 439–451.

(37)   Gillis, E. A. L.; Rajabi, K.; Fridgen, T. D. Structures of Hydrated Li+−Thymine and
        Li+−Uracil Complexes by IRMPD Spectroscopy in the N−H/O−H Stretching Region. *J.
        Phys. Chem. A* **2009**, *113*, 824–832.

(38)   Burt, M. B.; Fridgen, T. D. Gas-Phase Structures of Pb2+-Cationized Phenylalanine and
        Glutamic Acid Determined by Infrared Multiple Photon Dissociation Spectroscopy and
        Computational Chemistry. *J. Phys. Chem. A* **2013**, *117*, 1283–1290.

(39)   Rodgers, M. T.; Armentrout, P. B.; Oomens, J.; Steill, J. D. Infrared Multiphoton
        Dissociation Spectroscopy of Cationized Threonine: Effects of Alkali-Metal Cation Size
        on Gas-Phase Conformation. *J. Phys. Chem. A* **2008**, *112*, 2258–2267.

(40)   Mino Jr., W. K.; Szczepanski, J.; Pearson, W. L.; Powell, D. H.; Dunbar, R. C.; Eyler, J. R.;
        Polfer, N. C. Vibrational Signatures of Zwitterionic and Charge-Solvated Structures for
        Alkaline Earth-Tryptophan Dimer Complexes in the Gas Phase. *Int. J. Mass Spectrom.*
        2010, *297*, 131–138.

(41)   Dunbar, R. C.; Steill, J. D.; Oomens, J. Cationized Phenylalanine Conformations

Characterized by IRMPD and Computation for Singly and Doubly Charged Ions. *Phys. Chem. Chem. Phys.* **2010**, *12*, 13383–13393.

(42)   Bush, M. F.; O'Brien, J. T.; Prell, J. S.; Saykally, R. J.; Williams, E. R. Infrared Spectroscopy of Cationized Arginine in the Gas Phase: Direct Evidence for the Transition from Nonzwitterionic to Zwitterionic Structure. *J. Am. Chem. Soc.* **2007**, *129*, 1612–1622.

(43)   Forbes, M. W.; Bush, M. F.; Polfer, N. C.; Oomens, J.; Dunbar, R. C.; Williams, E. R.; Jockusch, R. A. Infrared Spectroscopy of Arginine Cation Complexes: Direct Observation of Gas-Phase Zwitterions. *J. Phys. Chem. A* **2007**, *111*, 11759–11770.

(44)   Carl, D. R.; Cooper, T. E.; Oomens, J.; Steill, J. D.; Armentrout, P. B. Infrared Multiple Photon Dissociation Spectroscopy of Cationized Methionine: Effects of Alkali-Metal Cation Size on Gas-Phase Conformation. *Phys. Chem. Chem. Phys.* **2010**, *12*, 3384–3398.

(45)   Drayß, M. K.; Armentrout, P. B.; Oomens, J.; Schäfer, M. IR Spectroscopy of Cationized Aliphatic Amino Acids: Stability of Charge-Solvated Structure Increases with Metal Cation Size. *Int. J. Mass Spectrom.* **2010**, *297*, 18–27.

(46)   Pearson, R. G. Hard and Soft Acids and Bases. *J. Am. Chem. Soc.* **1963**, *85*, 3533–3539.
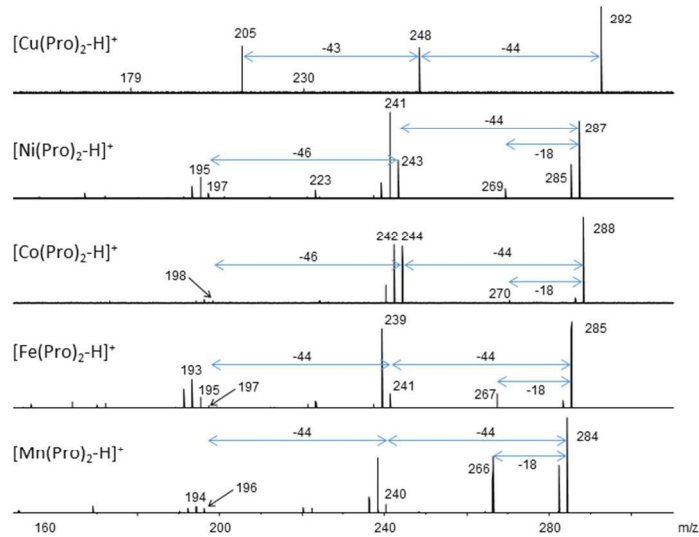
Figure 1. SORI/CID spectra obtained for [Mn(Pro)$_2$-H]$^+$, [Fe(Pro)$_2$-H]$^+$, [Co(Pro)$_2$-H]$^+$, [Ni(Pro)$_2$-H]$^+$ and [Cu(Pro)$_2$-H]$^+$.

254x190mm (96 x 96 DPI)
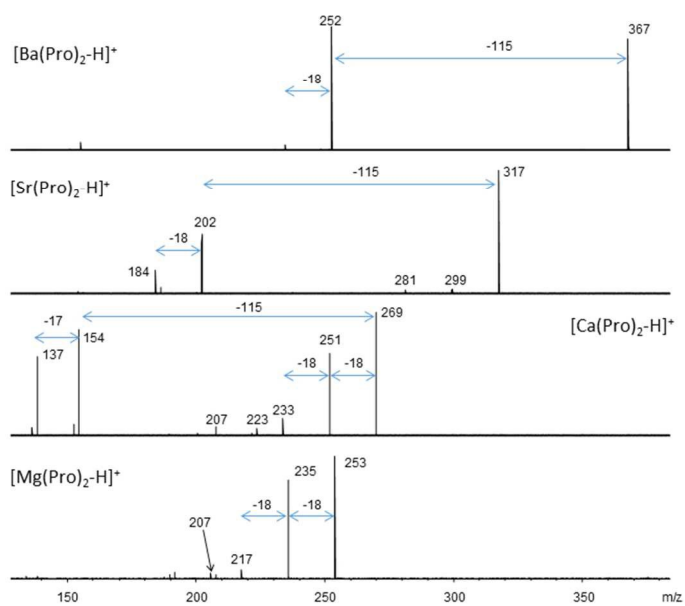
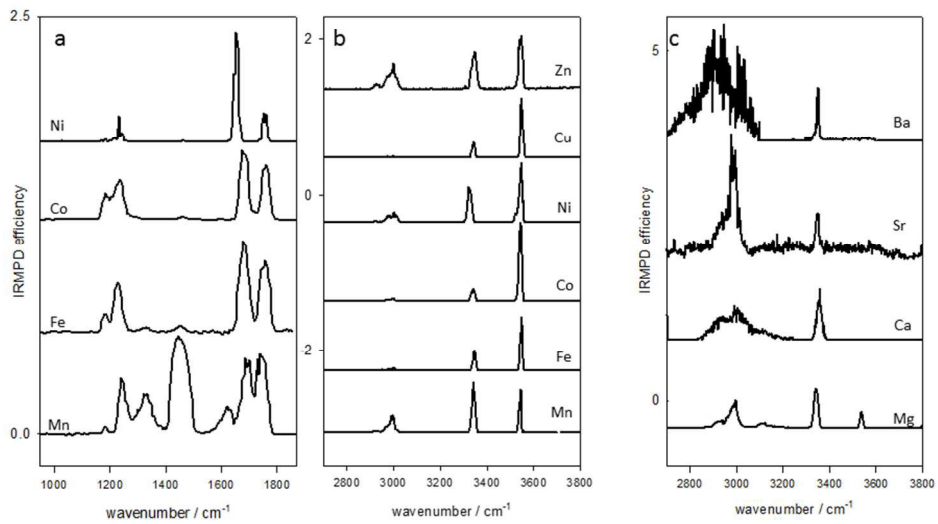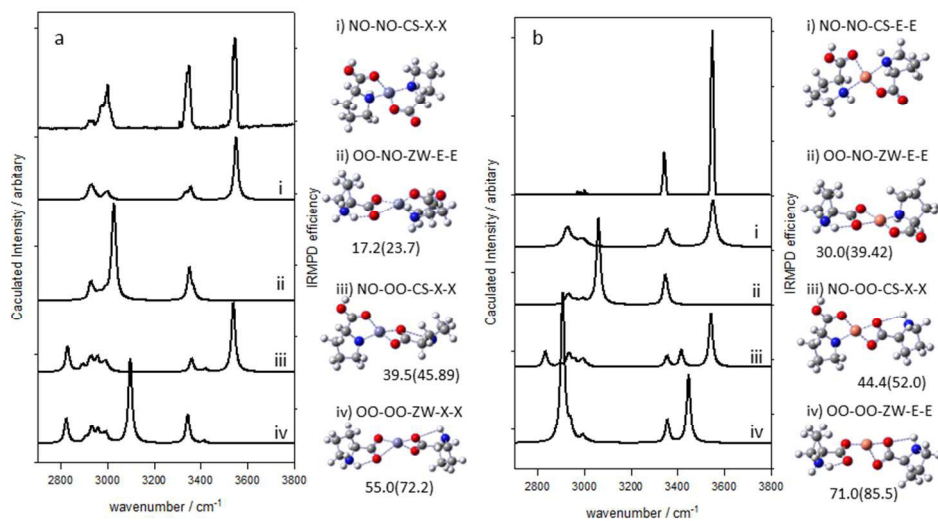**Figure 2.** SORI/CID spectra obtained for [Mg(Pro)₂-H]⁺, [Ca(Pro)₂-H]⁺, [Sr(Pro)₂-H]⁺, [Ba(Pro)₂-H]⁺.

254x190mm (96 x 96 DPI)

Figure 3. Comparison of the experimental IRMPD spectra (a) from 1000 to 1900 cm^{-1} where M = Mn, Fe, Co and Ni, (b) from 2700 to 3800 cm^{-1} where M = Mn, Fe, Co, Ni, Cu, Zn and (c) from 2800 to 3800 cm^{-1} where M = Mg, Ca, Sr and Ba.

254x190mm (96 x 96 DPI)

Figure 4. Comparison of the experimental IRMPD spectrum and calculated IR spectra of the lowest energy structures of each form of the a) $[Zn(Pro)_2-H]^+$ and b) $[Cu(Pro)_2-H]^+$ complexes in the 2700 to 3800 cm^{-1} region. Energies are B3LYPD3/6-311+G(3df3pd)//B3LYPD3/6-31+G(d,p) 298 K Gibbs energies (and enthalpies) and in kJ mol^{-1} and are relative to the lowest energy structure shown as i).
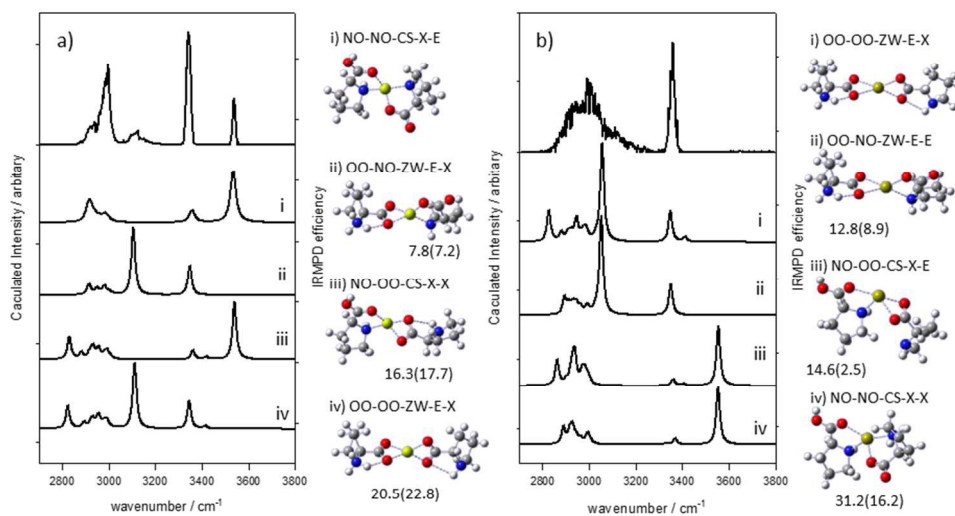
254x190mm (96 x 96 DPI)
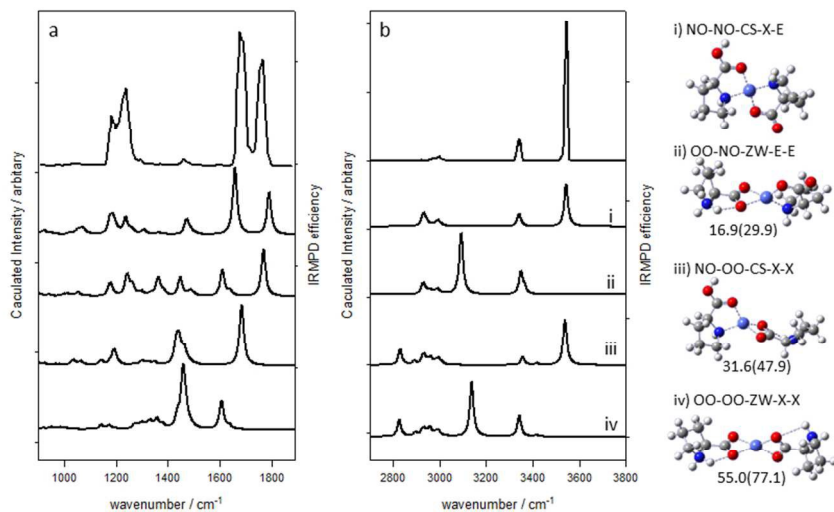
Fig. 5. comparison of the experimental IRMPD spectrum and calculated IR spectra of the lowest energy structures of each form of the $[Co(Pro)_2-H]^+$ in a) 1000 to 2000 cm^{-1} region and b) 2800 to 3800 cm^{-1} region. Energies are B3LYPD3/6-311+G(3df3pd)//B3LYPD3/6-31+G(d,p) 298 K Gibbs energies (and enthalpies) and in kJ mol^{-1} and are relative to the lowest energy structure shown as i).

254x190mm (96 x 96 DPI)
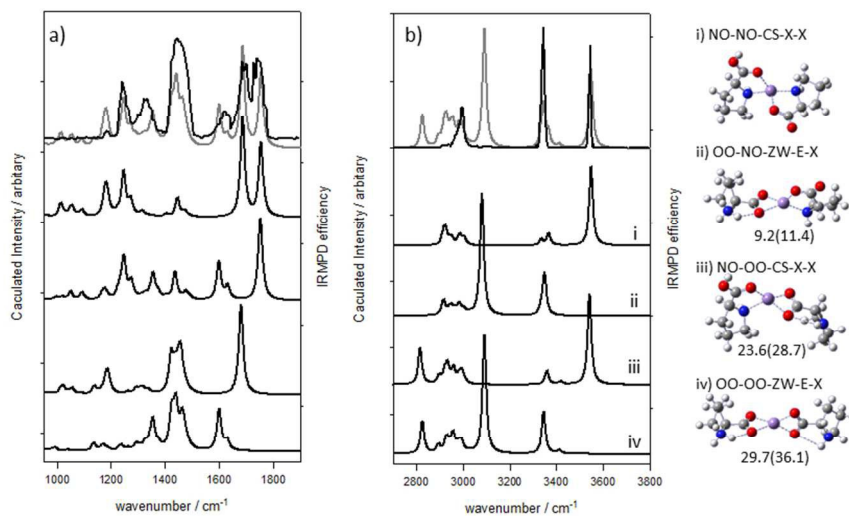
Fig. 6. Comparison of the experimental IRMPD spectrum and calculated IR spectra for the lowest energy structures of each form of the [Mn(Pro)$_2$ -H]$^+$ complex in the a) 1000 to 2000 cm^{-1} region and b) 2800 to 3800 cm^{-1} region. Energies are B3LYPD3/6-311+G(3df3pd)//B3LYPD3/6-31+G(d,p) 298 K Gibbs energies (and enthalpies) and in kJ mol^{-1} and are relative to the lowest energy structure shown as i). The grey line overlaying the experimental spectrum is a sum of complex i) and iv).

254x190mm (96 x 96 DPI)

Fig. 7. Comparison of the experimental IRMPD spectrum and calculated IR spectra for the lowest energy structures of each form of the a) [Mg(Pro)$_2$-H]$^+$, b) [Ca(Pro)$_2$-H]$^+$, c) [Sr(Pro)$_2$-H]$^+$, and d) [Ba(Pro)$_2$-H]$^+$ complexes in the 2700 to 3800 cm^{-1} region. Energies are B3LYPD3/6-311+G(3df3pd)//B3LYPD3/6-31+G(d,p) 298 K Gibbs energies (and enthalpies) and in kJ mol^{-1} except for Sr and Ba where the Def2TZVP basis sets were used and are relative to the lowest energy structure shown as i).
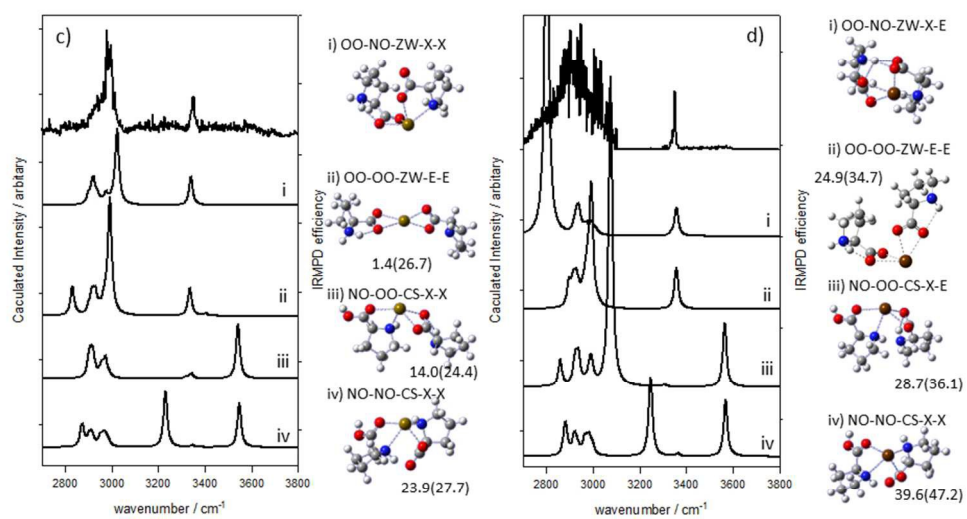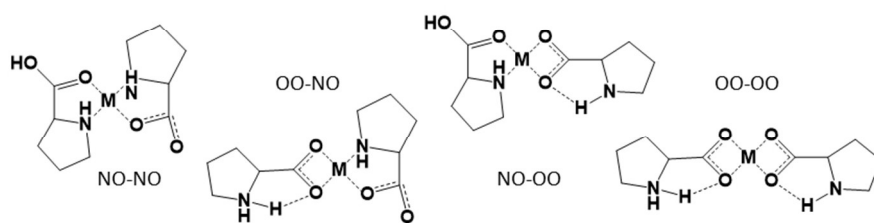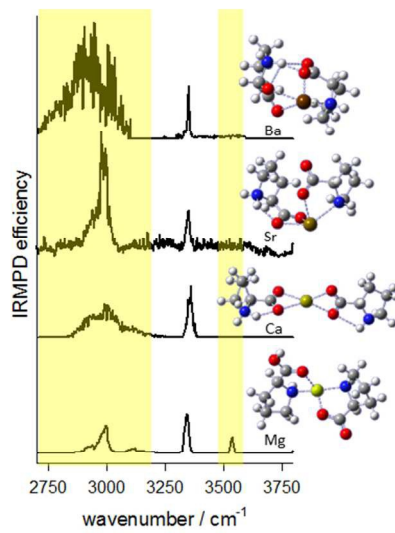
254x190mm (96 x 96 DPI)

Fig. 7. cont'd

254x190mm (96 x 96 DPI)

Scheme 1. The four main M(Pro$_2$-H)$^+$ structures.

254x190mm (96 x 96 DPI)

254x190mm (96 x 96 DPI)